Misalignment-Tolerant IPT Coupler with Enhanced Magnetic Flux Variation Suppression and Reduced Copper Usage

Hai Xu, Zhicong Huang, *Senior Member, IEEE*, Xiaolu Lucia Li, *Member, IEEE*, and Chi K. Tse, *Fellow, IEEE*

***Abstract*—Misalignment tolerance is essential in the design and implementation of inductive power transfer (IPT) systems. This paper proposes an IPT coupler, termed the rectangular-solenoidal pad (RSP), which combines a rectangular coil and a solenoidal coil. The proposed RSP can effectively capture both vertical and horizontal magnetic fields, complementing each other to suppress magnetic flux variation during misalignment. Compared with the commonly-used double D quadrature pad (DDQP), the proposed RSP achieves the same level of magnetic flux variation suppression with less coil wire, making it more misalignment-tolerant with the same amount of copper. To optimize the design for misalignment tolerance, a quick approximation method for designing the solenoidal coil is developed to eliminate the need to simulate mutual inductances across the entire range of misalignment during coil design. A 1-kW experimental prototype is built to validate the proposed design.**

***Index Terms*—Inductive power transfer, misalignment tolerance, coupler design, magnetic flux compensation.**

I. Introduction

In recent years, the adoption of electric vehicles (EVs) has gained significant momentum as part of the global effort to promote sustainable and environmentally friendly transportation. However, the traditional conductive charging method for EVs is cumbersome and carries potential risks. In response to these challenges, inductive power transfer (IPT) technology has emerged as an attractive solution, enabling the wireless transfer of power through magnetic coupling without the need for physical contact [1]–[3]. IPT offers several advantages, including user-friendly and maintenance-free operations, positioning it as a promising alternative for EV charging [4], [5]. Despite its numerous advantages, misalignment between the transmitter (Tx) pad and the receiver (Rx) pad remains a persistent issue that adversely affects power transfer efficiency and overall system performance [6]. Consequently, enhancing the tolerance to misalignment becomes paramount in the design and implementation of IPT systems.

Magnetic couplers, comprising a Tx pad and a Rx pad, are the essential components in an inductive power transfer (IPT) system and play a significant role in tolerating misalignment. Therefore, considerable effort has been devoted to study the inherent capability of an IPT system against pad misalignment in the coupler. The symmetric design of magnetic couplers, i.e., a pair of CPs [7], [8] or DDPs [9], [10] with identical parameters, is susceptible to misalignment due to the significant variation in magnetic flux distribution. To mitigate the variation in magnetic flux distribution and enhance the misalignment tolerance, some studies have been carried out to optimize various parameters of the magnetic coupler. These parameters usually include the turn number, turn spacing, ferrite shape, and internal and external diameters, and so on [11]–[15]. For instance, the study proposed by Rituraj *et al.* [15] focuses on the arrangement method for the RP, and the study proposed by Budhia *et al.* [16] optimizes the core layout and shape of CP to improve the overall coupling effectiveness. A new symmetric coupler has been proposed that connects circular and rectangular coils in series to form a single coil to enhance the coupling coefficient compared with the standard CP and RP at optimum coil widths and number of turns [17]. However, these methods can only provide limited mitigation of the variation in magnetic flux distribution and symmetric magnetic couplers still face challenges related to the misalignment. A straightforward approach to enhance the misalignment tolerance is to strive for a nearly uniform magnetic flux distribution by employing an asymmetric design. This involves using a Tx pad with an area several times larger than that of the Rx pad. The design by Al Mahmud *et al.* [18] configures multiple rectangular coils into a large rectangular plane to form a Tx planar structure generating a nearly-uniform magnetic field for compensating pad misalignment. However, suppressing the circulating current is a significant issue because of the cross coupling between the multiple coils. To bridge this gap, a self-decoupled and integrated multiple coil set has been designed, which however is too complex and difficult to implement [19]. Besides, the associated drive and control design is too complex to precisely activate the individual coils for these multiple coils planar solutions.

To simplify the control, the Tx pad can also be designed as a single coil. For example, in a dynamic wireless EV charging system, the Tx pad can be in the form of a long track to generate a nearly uniform magnetic flux distribution

Manuscript received 31 December 2023; revised 28 February 2024; accepted 30 March 2024. This work is supported by the Science and Technology Planning Project of Guangdong Province (2023A0505050124), the Natural Science Foundation of Guangdong Province (2023A1515011623), and Hong Kong RGC Theme-Based Research Scheme Project T23-701/20R. (Corresponding author: Zhicong Huang and Xiaolu Lucia Li)

Hai Xu and Zhicong Huang are with the Shien-Ming Wu School of Intelligent Engineering, South China University of Technology, Guangzhou, 510006, China (e-mail: wixuh@mail.scut.edu.cn, zhiconghuang@scut.edu.cn).

Xiaolu Lucia Li and Chi K. Tse are with the Department of Electrical Engineering, City University of Hong Kong, Hong Kong, China (email: luciali@ieee.org, cktse@ieee.org)

Digital Object Identifier TXXXxxxx.0000.0000.0000

along the track [20]. Also, an optimal design method for the DD coil, which uses a Tx DD coil that doubles the size of the Rx DD coil to achieve a high coupling coefficient at the offset condition, has been investigated [21]. However, such asymmetric design results in degrading the overall coupling of the magnetic couplers, and thus a trade-off between the power control and power efficiency is inevitable [22].

In the absence of a Tx pad generating a nearly uniform magnetic field, an approach is to design a coupler based on mutual cancellation mechanism [23]–[26], which connects multi-unipolar coils in anti-series on the Tx or Rx side to offer a constant mutual inductance difference over the entire pad misalignment profile. An anti-series rectangular coil and circular coil pad on the Tx pad is used to sustain a nearly steady mutual inductance difference that fits the pad misalignment [23]. The design including four rectangular coils in an inverse series at the Tx side to compensate for the pad misalignment has been presented by Zhang *et al.* [24]. Since the four coils are in anti-series connection with some others, the variation is cancelled out, resulting in a consistent magnetic field despite the misalignment. However, it should be noted that the cancellation of the magnetic field in this way may weaken the power transfer capacity and require more copper usage to construct the magnetic pad. Furthermore, cross-coupling and complex design becomes inevitable due to the layout of multi-anti-series coils on the same side. Another approach is to construct a Rx pad with hybrid coil structures based on a mutual complementary strategy. It is generally known that the unipolar magnetic pads facilitate the capture of the vertical magnetic field, while bipolar magnetic pads help the capture of the horizontal magnetic field. The complementary concept of this Rx pad is illustrated in Fig. 1. Under misalignment conditions, the capture of the vertical magnetic flux may decrease, while the capture of the horizontal magnetic flux increases, or vice versa. The double-D quadrature pad (DDQP), which consists of a rectangular pad in quadrature with a double-D pad (DDP), has been widely adopted ever since its proposal [27]–[29]. Given the Tx pad generating a unipolar magnetic field and in the case of misalignment, the RP captures less vertical magnetic field, while the DDP captures more horizontal magnetic field. Proper parameter design of the DDQP has also been studied to ensure the variations in the captured vertical and horizontal magnetic field are complementary, thereby enabling stable power transfer against misalignment [27]. However, in order to capture the horizontal magnetic flux, the DD coil needs to encompass the entire area of the coupler. This results in an excessive consumption of copper resources, which is not a practical and effective solution. Thus, it can be observed that the traditional symmetric design cannot tolerate pad misalignment, while some asymmetric designs have the capability of misalignment tolerance but suffer from increased copper usage, reduced coupling coefficient and cross-coupling issues.

To address the aforementioned issue, this paper proposes an Rx coupler that combines a rectangular coil and a solenoidal coil, referred to as rectangular-solenoidal pad (RSP). The proposed magnetic coupler can effectively capture both vertical and horizontal magnetic fields in a complementary manner.

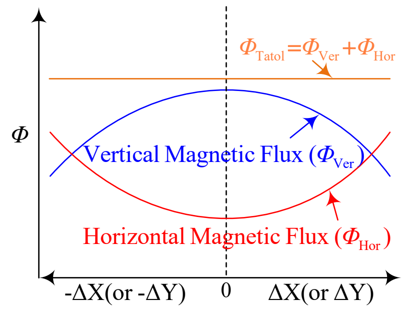

Fig. 1. Complementary design concept.

During the misalignment, the solenoidal coil is more advantageous in capturing the horizontal magnetic field to compensate for the decrease of the vertical magnetic field captured by the rectangular coil. In comparison to the DDQP coupler, the proposed RSP coupler can achieve similar coupling performance while requiring less coil wire, meaning that it has better misalignment tolerance with the same amount of copper. To optimize the design for misalignment tolerance, a quick approximation method for designing the solenoidal coil is developed. It enables efficient determination of the optimal design and eliminates the need to simulate mutual inductances across the entire range of misalignment during coil design. The novelties and contributions of this paper are summarized as follows:

1) This paper proposes rectangular-solenoidal pad (RSP) coupler that combines a rectangular coil and a solenoidal coil to effectively capture both vertical and horizontal magnetic fields in a complementary manner for minimizing the effect of pad misalignment.
2) In comparison to the conventional double-D-quadrature pad (DDQP) coupler, the proposed design can achieve similar coupling performance while requiring less coil wire, thus achieving better misalignment tolerance with the same amount of copper.
3) To optimize the design for misalignment tolerance, a quick approximation method for designing the solenoidal coil is developed to facilitate fast determination of the optimal design parameters and eliminate the need to simulate mutual inductances across the entire range of misalignment during coil design.

The rest of this paper is organized as follows. Section II presents the proposed RSP coupler and highlights the advantages of magnetic flux capture capability of the solendial coil in comparison to the DD coil. In Section III, a quick approximation method for designing the solenoidal coil is developed, and the copper usage is shown to be significantly reduced compared with the DD coil. Section IV experimentally validates the proposed design. Finally, Section V concludes the paper.

II. Proposed Rectangular-Solenoidal Pad

A. Operating Principle

Fig. 2 depicts the proposed Rx pad with complementary magnetic field capture capability. It comprises a rectangular

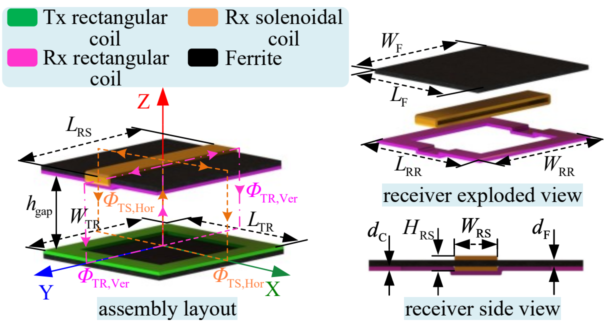

Fig. 2. Proposed rectangular-solenoidal pad (RSP).

pad and a solenoidal pad, which are designed to separately capture the vertical and horizontal components of the magnetic field generated by the Tx rectangular pad. These two pads exhibit no cross-coupling effect because they capture magnetic fields in perpendicular directions.

As highlighted in Fig. 2, the vertical magnetic flux captured by the Rx rectangular pad is donated as $\Phi_{\text{TR,Ver}}$, while the horizontal magnetic flux captured by the Rx solenoidal pad is indicated as $\Phi_{\text{TS,Hor}}$. Both $\Phi_{\text{TR,Ver}}$ and $\Phi_{\text{TS,Hor}}$ represent the components of the magnetic flux in normal directions, and their magnitudes and polarities are dependent on the specific misalignment conditions. The effective magnetic flux captured by the overall RSP can be defined as the sum of the absolute values of $\Phi_{\text{TR,Ver}}$ and $\Phi_{\text{TS,Hor}}$, as given by

$$|\Phi_{\text{RSP}}| = |\Phi_{\text{TR,Ver}}| + |\Phi_{\text{TS,Hor}}|. \tag{1}$$

According to Neumann formula, the mutual inductance between the Tx rectangular pad and the RSP is given by

$$|M_{\text{RSP}}| = \frac{|\Phi_{\text{RSP}}|}{I_{\text{T}}} = |M_{\text{TR}}| + |M_{\text{TS}}|, \tag{2}$$

where I_{T} is the excitation current of the Tx rectangular pad.

It is known that the magnetic flux $\Phi_{\text{TR,Ver}}$ traversing the rectangular pad of the RSP will be weakened under various misalignments along the X-axis. The red solid curve in Fig. 3(f) indicates the trend of $|\Phi_{\text{TR,Ver}}|$ along with the X-misalignment direction. It can be observed that $|\Phi_{\text{TR,Ver}}|$ decreases with the increase of misalignment. On the other hand, the FEA results shown in Fig. 3(a)–(d) illustrate the distribution of $\Phi_{\text{TS,Hor}}$ across the solenoidal coil of the RSP for various X-misalignments. It can be observed that the X component of magnetic flux density $\boldsymbol{B}_{\text{X}}$ traversing the receiver solenoidal coil increases with an increase of offset distance. In other word, it indicates an increase in horizontal magnetic flux with a rise in misalignment. Therefore, in contrast to the trend of variation of $|\Phi_{\text{TR,Ver}}|$, $|\Phi_{\text{TS,Hor}}|$ increases with the increase of misalignment, as shown by the orange dashed curve of $|\Phi_{\text{TS,Hor}}|$ in Fig. 3(f). Given the above observations, if the variations of $|\Phi_{\text{TR,Ver}}|$ and $|\Phi_{\text{TS,Hor}}|$ are complementary by employing appropriate designs of the rectangular and solenoidal pads, the proposed RSP can indeed possess misalignment tolerance capability.

B. Calculation of Magnetic Flux

With a transmitter consisting of a single unipolar rectangular coil, the magnetic field it generates is aligned vertically. Employing the coordinate system depicted in Fig. 4 and adhering to the Biot-Savart law, the magnetic flux density at point P can be determined for a rectangular coil with N turns as follows:

$$\begin{aligned}\boldsymbol{B} = \frac{\mu_0 I}{4\pi}\sum_{\text{i}=1}^{N}\Big(&\int_{Ai}^{Bi}\frac{dl\times\widehat{\boldsymbol{r}_{1i}}}{r_{1i}^2}+\int_{Bi}^{Ci}\frac{dl\times\widehat{\boldsymbol{r}_{2i}}}{r_{2i}^2}\\&+\int_{Ci}^{Di}\frac{dl\times\widehat{\boldsymbol{r}_{3i}}}{r_{3i}^2}+\int_{Di}^{Ai}\frac{dl\times\widehat{\boldsymbol{r}_{4i}}}{r_{4i}^2}\Big).\end{aligned} \tag{3}$$

In this equation, $\boldsymbol{r}_i$ denotes the relative position vector from point P to the current element dl, while $\widehat{\boldsymbol{r}_i}$ represents the unit vector of $\boldsymbol{r}_i$. Notably, bold italics signify vectors unless stated otherwise.

Given that magnetic flux density $\boldsymbol{B}$ is a spatial vector, Equation (3) implies that $\boldsymbol{B}$ can also be articulated in terms of its X, Y, and Z components, as presented below:

$$\boldsymbol{B} = \sum_{\text{i}=1}^{N}(\boldsymbol{B}_{\text{Xi}} + \boldsymbol{B}_{\text{Yi}} + \boldsymbol{B}_{\text{Zi}}). \tag{4}$$

The amplitude of $\boldsymbol{B}$ is calculated by

$$B = \sqrt{(\sum_{\text{i}=1}^{N}\boldsymbol{B}_{\text{Xi}})^2 + (\sum_{\text{i}=1}^{N}\boldsymbol{B}_{\text{Yi}})^2 + (\sum_{\text{i}=1}^{N}\boldsymbol{B}_{\text{Zi}})^2}. \tag{5}$$

Subsequently, the total magnetic flux traversing the enclosed surface can be calculated using the equation:

$$\Phi = \int_S B\cos\alpha\, dS. \tag{6}$$

Here, α represents the angle between the enclosed surface and the magnetic flux density vector $\boldsymbol{B}$.

As discussed in Section I and elaborated in Section II-A, both the proposed RSP and the commonly-used DDQP (as shown in Fig. 5) demonstrate misalignment tolerance capability. The proposed RSP is intended to reduce copper usage while maintaining the same misalignment tolerance capability as the commonly-used DDQP. Thus, a comparative study between the RSP and the DDQP will be conducted subsequently. Although these couplers share the usage of an identical rectangular pad for capturing vertical magnetic flux under well-aligned conditions, they diverge in their approaches to achieving misalignment tolerance. To provide specifics, the proposed RSP employs a solenoidal coil to capture horizontal magnetic flux for complementary compensation, while the commonly-used DDQP employs a DD coil. To quantitatively compare these two designs, calculations are undertaken to determine the magnetic flux captured by the solenoidal coil and the DD coil, as detailed in the following.

For the RSP coupler, as depicted in Fig. 2, the resultant magnetic flux experienced by the solenoidal coil corresponds to the integral of the magnetic flux density $\boldsymbol{B}_{\text{X}}$ of the X component over the effective enclosed surface. Consequently, based on (5) and (6), the effective magnetic flux harnessed

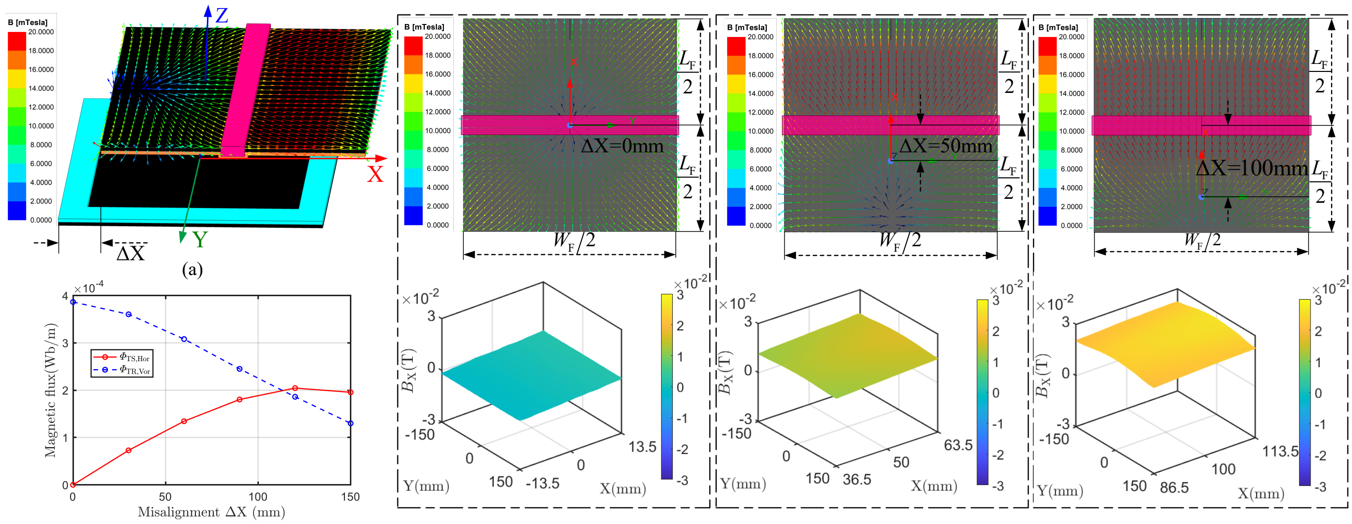

Fig. 3. Magnetic flux density distribution traversing solenoidal coil of RSP coupler under various misalignments along the X-axis, (a) coordinates, (b) $\Delta X = 0$ mm (fully aligned), (c) ΔX=50 mm, (d) ΔX=100 mm, (f) diagrams of $\Phi_{\mathrm{TR,Ver}}$ and $\Phi_{\mathrm{TS,Hor}}$

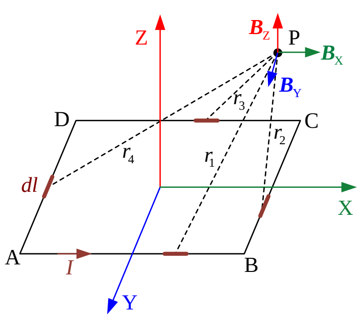

Fig. 4. Coordinates for the calculation of magnetic flux density with Biot-Savart law.

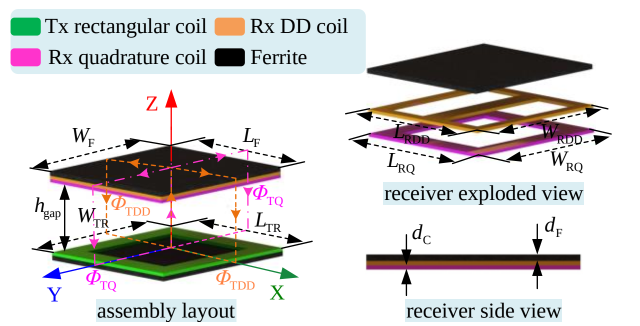

Fig. 5. Commonly-used double-D-quadrature pad (DDQP).

by the solenoidal coil, which is wound with N_{S} turns, can be mathematically represented as:

$$\Phi_{\mathrm{TS,Hor}} = \int_{S_1} B_{\mathrm{X}_{\mathrm{S}_1}} \cos\alpha dS + \int_{S_2} B_{\mathrm{X}_{\mathrm{S}_2}} \cos\alpha dS + \cdots + \int_{S_{\mathrm{i}}} B_{\mathrm{X}_{\mathrm{S}_{\mathrm{i}}}} \cos\alpha dS + \cdots + \int_{S_{N_{\mathrm{S}}}} B_{\mathrm{X}_{\mathrm{SN}_{\mathrm{S}}}} \cos\alpha dS. \tag{7}$$

In this equation, S_{i} represents the effective area of the i^{th} turn of the solenoidal coil, which captures the magnetic flux density of the X component denoted as $B_{\mathrm{X_{Si}}}$. Due to the uniformity of the effective area for each turn of the solenoidal coil, the equation can be simplified to:

$$S_{\mathrm{S}} = S_1 = S_2 = \cdots = S_{N_{\mathrm{S}}} = (L_{\mathrm{RS}} - 2d_{\mathrm{C}})(H_{\mathrm{RS}} - 2d_{\mathrm{C}}), \tag{8}$$

where L_{RS}, H_{RS} is the length and height of solenoidal coil respectively, and d_{C}, P_{N} is corresponding to litz wire diameter and turn spacing, as depicted in Fig. 2 and Fig. 6(b). Therefore, the (7) can be rewriten as

$$\Phi_{\mathrm{TS,Hor}} = \sum_{\mathrm{i}=1}^{N_{\mathrm{S}}} \int_{S_{\mathrm{S}}} B_{\mathrm{X}_{\mathrm{S}_{\mathrm{i}}}} \cos\alpha dS. \tag{9}$$

In the case of the DDQP coupler depicted in Fig. 5, the effective magnetic flux coupled with the DD coil is acquired by integrating the Z component, i.e., $\boldsymbol{B}_{\mathrm{Z}}$, of the magnetic flux density over the effective enclosed surface. Nevertheless, due to the opposing direction of winding on the left and right sides of the DD coil, the overall magnetic flux coupled with the DD coil consisting of N_{D} turns is the difference between that through the left side (i.e., $\boldsymbol{B}_{\mathrm{Z_L}}$) and the right side (i.e., $\boldsymbol{B}_{\mathrm{Z_R}}$). This can be expressed as:

$$\Phi_{\mathrm{TDD}} = \int_{S_{\mathrm{L}_1}} B_{\mathrm{Z}_{\mathrm{L}_1}} \cos\alpha dS + \cdots + \int_{S_{\mathrm{L}_{N_{\mathrm{D}}}}} B_{\mathrm{Z}_{\mathrm{L}_{N_{\mathrm{D}}}}} \cos\alpha dS - \left(\int_{S_{\mathrm{R}_1}} B_{\mathrm{Z}_{\mathrm{R}_1}} \cos\alpha dS + \cdots + \int_{S_{\mathrm{R}_{N_{\mathrm{D}}}}} B_{\mathrm{Z}_{\mathrm{R}_{N_{\mathrm{D}}}}} \cos\alpha dS\right). \tag{10}$$

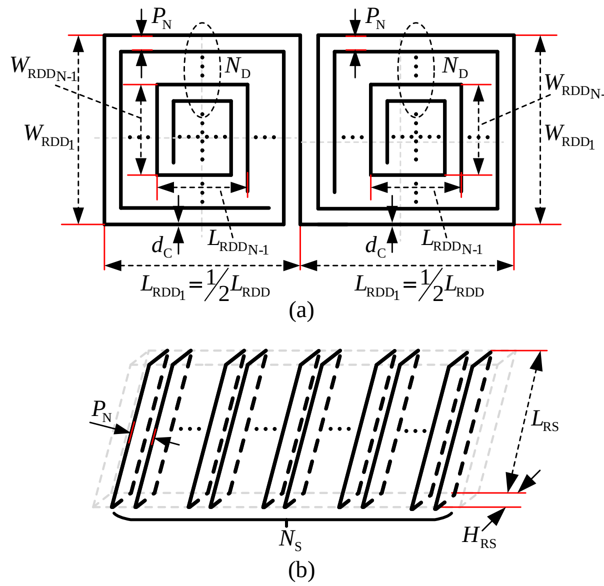

Fig. 6. Geometries of (a) the solenoial coil and (b) the DD coil.

Given that the DD coil is symmetrical, as depicted in Fig.5 and Fig. 6(a), $S_{\mathrm{DD_i}}$ can be equivalent to $S_{\mathrm{L_i}}$ and $S_{\mathrm{R_i}}$. Hence, (10) can be reformulated as follows:

$$\begin{aligned}\Phi_{\mathrm{TDD}} = &\sum_{i=1}^{N_{\mathrm{D}}} \int_{S_{\mathrm{DD_i}}} B_{\mathrm{Z_{L_i}}} \cos\alpha dS \\ &- \sum_{i=1}^{N_{\mathrm{D}}} \int_{S_{\mathrm{DD_i}}} B_{\mathrm{Z_{R_i}}} \cos\alpha dS,\end{aligned} \tag{11}$$

where

$$\begin{aligned} S_{\mathrm{DD_1}} =& \frac{1}{2} L_{\mathrm{RDD}} W_{\mathrm{RDD}} \\ S_{\mathrm{DD_2}} =& (\frac{1}{2} L_{\mathrm{RDD}} - 2(d_{\mathrm{C}} + P_{\mathrm{N}}))(W_{\mathrm{RDD}} - 2(d_{\mathrm{C}} + P_{\mathrm{N}})) \\ &\dots \\ &\dots \\ S_{\mathrm{DD_N}} =& (\frac{1}{2} L_{\mathrm{RDD}} - 2(N_{\mathrm{D}} - 1)(d_{\mathrm{C}} + P_{\mathrm{N}}))(W_{\mathrm{RDD}} - \\ & 2(N_{\mathrm{D}} - 1)(d_{\mathrm{C}} + P_{\mathrm{N}})). \end{aligned} \tag{12}$$

L_{RDD} is the length of DD coil while W_{RDD} is corresponding width.

C. Analysis of Magnetic Flux Capture Capability

Based on the calculation of magnetic flux given in Section II-B, a quantitative comparison of the proposed RSP and the DDQP can be conducted. As shown in Figs. 2 and 5, a rectangular pad is used to generate a unipolar magnetic field on the Tx side, while the RSP and DDQP are on the Rx side. The following assumptions are made for the analysis:

1) The rectangular (quadrature) coils of the RSP and DDQP are symmetric to the Tx rectangular coil, which means the RSP and DDQP have identical magnetic flux capture capability in the absence of misalignment.
2) The turn spacing P_{N} is set to zero in order to simplify both the fabrication process and the analysis of the coupler.
3) The Tx side has the same excitation current I_{T}, which is fixed at 10 A.

TABLE I
PARAMETERS OF THE COUPLER

Items	Symbols	Parameters	Value(mm)
RSP coupler	L_{RR}	Lenght of Rx rectangular coil	300
	W_{RR}	Width of Rx rectangular coil	300
	L_{RS}	Lenght of Rx solenoidal coil	306
	H_{RS}	Height of Rx solenoidal coil	9
DDQP coupler	L_{RDD}	Lenght of Rx DD coil	300
	W_{RDD}	Width of Rx DD coil	300
	L_{RQ}	Lenght of Rx solenoidal coil	300
	W_{RQ}	Width of Rx quadrature coil	300
Shared parameters	L_{TR}	Lenght of Tx rectangular coil	300
	W_{TR}	Width of Tx rectangular coil	300
	L_{F}, W_{F}	Ferrite dimensions	300,300
	d_{F}		3
	d_{C}	Litz wire diameter of coils	3
	h_{gap}	Power transfer gap distance	60
	N	Turn numbers of unipolar coils	10
	P_{N}	Turn space of coils	0

Table I gives detailed parameters of the RSP and DDQP for the analysis of magnetic flux capture capability and copper usage. With (9) and (11), the effective magnetic flux coupled by solenoidal coil and DD coil can be calculated, if the magnetic flux density as well as the corresponding acceptance area can be obtained. Since the magnetic flux distribution is not uniform, the Finite Element Method (FEM) simulation is employed to determine the magnetic flux values. It is noteworthy that the proposed calculation is suitable for magnetic couplers either with or without magnetic ferrites.

To ensure a fair comparison of the magnetic flux capture capability, it is important to maintain the same amount of copper usage for both the solenoidal coil of the RSP and the DD coil of the DDQP. This allows for an accurate assessment of their respective performance without the influence of differing copper quantities. Without loss of generality, the copper usage is set at 5670 mm for both the solenoidal coil of the RSP and the DD coil of the DDQP to analyze the magnetic flux capture capability. The structures shown in Figs. 2 and 5 are considered. Unless specified, the following analysis is based on the parameters given in Table I. The solenoidal coil and DD coil can be wound to approximately 9 turns and 4 turns, respectively. Fig. 7(a) shows the numerically calculated results of the effective magnetic flux captured by the solenoidal coil and the DD coil under identical copper usage (5670 mm), at varying misalignment distances along the x-axis direction. The trends depicted in Fig. 7(a) show an increasing effective magnetic flux captured by both coils within a specific range of misalignments. Notably, the total effective flux captured by the proposed solenoidal coil exceeds that of the DD coil, implying that the solenoidal coil of the proposed design exhibits an improved magnetic flux capture capability. This enhancement makes it more advantageous for compensating the magnetic flux variation of the rectangular coil due to misalignment.

Furthermore, by using the data from Fig.7(a) and the

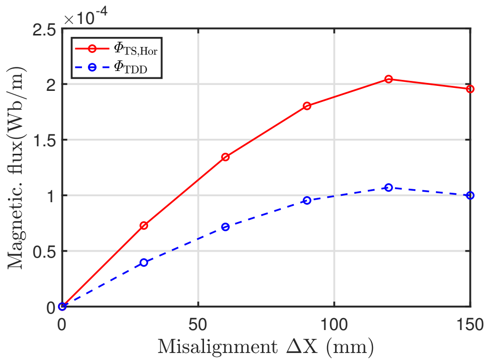

(a)

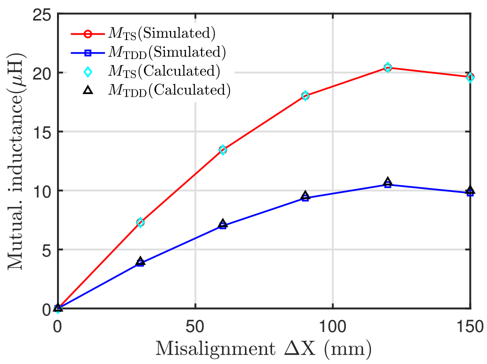

(b)

Fig. 7. (a) Numerically calculated results of the effective magnetic flux captured by the solenoidal coil and the DD coil ($\Phi_{\mathrm{TS,Hor}}$, Φ_{TDD}) and (b) corresponding mutual inductances versus misalignment distances along the X-axis direction.

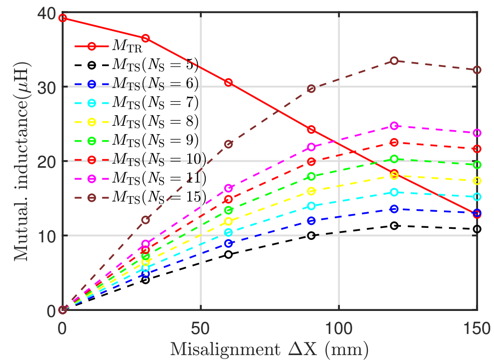

(a)

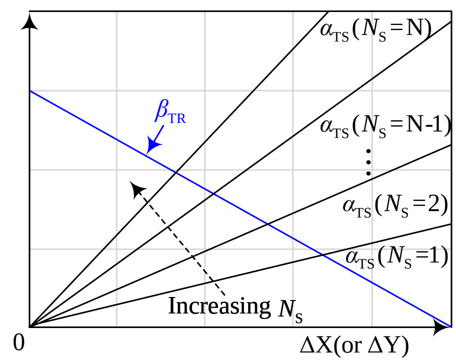

(b)

Fig. 8. (a) Mutual inductances M_{TR}, M_{TS}, and (b) approximate slope matching design principles of the proposed coupler with RSP under various misalignments along X-axis versus N_{S}.

relationship presented in (2), the mutual inductance performance of the solenoidal coil and DD coil with respect to the transmitter rectangular coil can be calculated, as illustrated in Fig.7(b). Obviously, the calculated mutual inductance for solenoidal coil (marked with "◊") and DD coil (marked with "△") aligns closely with the corresponding FEA simulation results (marked with "–◯–" and "–□–" respectively). This confirms the validity of the computational approach for the analysis.

III. Misalignment Tolerance Design and Analysis of Copper Usage

A. Misalignment Tolerance Design Using Approximate Slope Prediction

To enhance the misalignment tolerance capability of the proposed IPT coupler, it is essential to ensure that the overall mutual inductance M_{RSP} between the RSP and the Tx rectangular pad as given by (2) remain as consistent as possible within a range of misalignments. One significant factor that affects the coupling effect of the IPT coupler is the number of turns in the coil. Given that the coupler's structure and outer dimensions are fixed based on the design recommendations in SAE J2954 [30], this part of the study focuses on a design method to improve the offset tolerance by adjusting the solenoidal coil of the proposed RSP IPT coupler. In this design approach, we concentrate on modifying the number of turns (N_{S}) in the solenoidal coil. The variation of the simulation step for the number of turns is set to be 1 turn. By systematically adjusting the number of turns, we can assess the impact on the coupling effect and stability of mutual inductances under different misalignment conditions.

TABLE II
Slope and Copper Consumption of RSP Coupler and DDQP Coupler Versus Number of Turns

Symbol	Turns number	Slopes	Copper (mm)
Rectangular coil	10	-0.174	
Solenoidal coil	5	0.094	3150
	6	0.113	3780
	7	0.132	4410
	8	0.150	5040
	9	0.169	5670
	10	0.188	6300
	11	0.206	6930
	15	0.279	9450
DD coil	5	0.139	8520
	6	0.163	10080
	7	0.186	11592
	8	0.208	13056
	9	0.228	14472
	10	0.248	15840
	11	0.265	17160
	15	0.320	21960

Fig. 8(a) shows the simulation results of mutual inductance for the proposed RSP coupler versus misalignment distances when the solenoidal coil has different numbers of turns, donated as N_{S}. The mutual inductance between the solenoidal coil and the Tx rectangular coil is defined as complementary

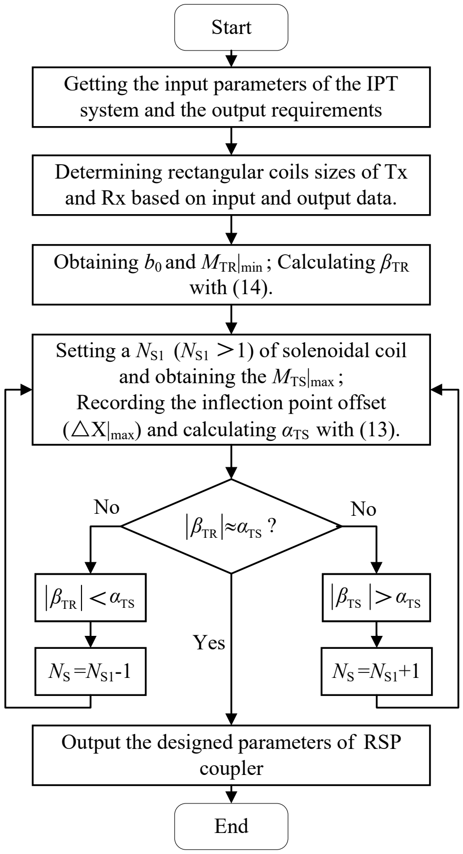

Fig. 9. Misalignment enhancement design flowchart based on approximate slope prediction of RSP coupler.

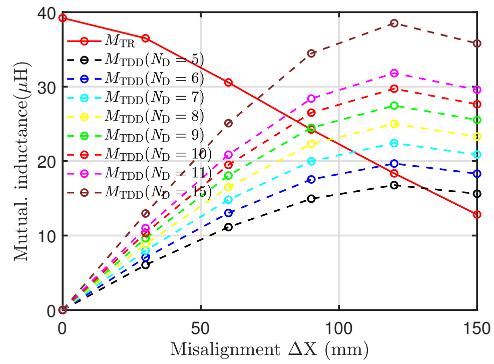

Fig. 10. Mutual inductances M_{TR}, M_{TDD} of the coupler with double-D-quadrature pad (DDQP) under various misalignments along X-axis versus N_D.

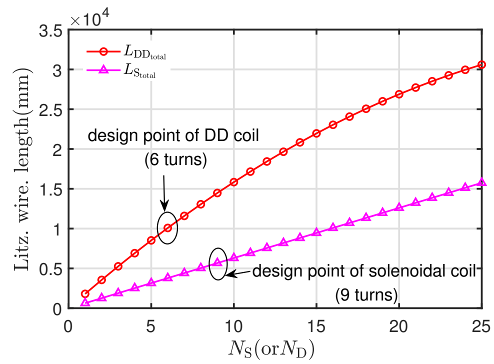

Fig. 11. Total wire length of solenoidal coil and DD coil versus N_S (or N_D).

mutual inductance and given by M_{TS}. As N_S increases in the solenoidal coil, M_{TS} also increases under misalignment conditions. It can be observed that the complementary mutual inductance M_{TS} demonstrates a non-monotonic behavior with increasing misalignment, showing an initial increase followed by a subsequent decrease. The inflection points of this behavior occur at the same position for various turn number N_S. For instance, the inflection point in the proposed design locates at a misalignment distance of $\Delta X|_{max} = 120$ mm, which is about 40% of the coupler size. Nevertheless, before reaching the maximum value, the compensation mutual inductance (M_{TS}) exhibits an approximately linear relationship with the misalignment, as illustrated in Fig.8(b). Therefore, the relationship between M_{TS} and the misalignment (ΔX) can be expressed by a linear equation as given by

$$M_{TS} \approx \alpha_{TS}\Delta X \tag{13}$$

where $\alpha_{TS} = \frac{M_{TS}|_{max}}{\Delta X|_{max} - \Delta X|_{min}}$ is the slope, (0, $M_{TS}|_{max}$) and (0, $\Delta X|_{max}$) are the ranges of complementary mutual inductance and the corresponding misalignment offset respectively.

As evident from the solid red curve in Fig. 8(a), the mutual inductance M_{TR} between the rectangular coil of the proposed RSP and the Tx rectangular coil diminishes as the misalignment offset increases. As illustrated in Fig.8(b), the curve can also be modeled in linear form and described by

$$M_{TR} \approx \beta_{TR}\Delta X + b_0 \tag{14}$$

where β_{TR} is a negative slope and b_0 represents the initial value of M_{TR} without misalignment. Based on (13) and (14), to achieve nearly constant magnetic flux against misalignment, α_{TS} and β_{TR} should be opposite to each other, leading to the following design criteria:

$$M_{TR} + M_{TS} \approx b_0, \text{ if} \tag{15}$$

$$\alpha_{TS} + \beta_{TR} = 0. \tag{16}$$

The value of β_{TR} is primarily determined by the design of the rectangular coil, which holds responsibility for power transfer and is typically fixed. On the other hand, α_{TS} can be designed by adjusting the turn number N_S of the solenoidal coil. It is noteworthy that the derivation of α_{TS} only necessitates knowledge of $M_{TS}|_{max}$, which occur at $\Delta X = 120$ mm. As a result, it is not necessary to simulate the mutual inductances across the entire range of misalignment. A comprehensive design procedure can be illustrated by the flowchart in Fig. 9. In the proposed design, β_{TR} is about -0.174. By performing finite element analysis, the values of $M_{TS}|_{max}$ corresponding to different values of N_S can be obtained. Using the data in Fig. 8(a), the values of the slope α_{TS} versus the turn number N_S can be calculated and summarized in Table II. It is easy to determine that by configuring the solenoidal coil with 9 turns, α_{TR} can be approximately set to 0.169. This choice of turns is the most optimal as it closely aligns with the criterion described in (16).

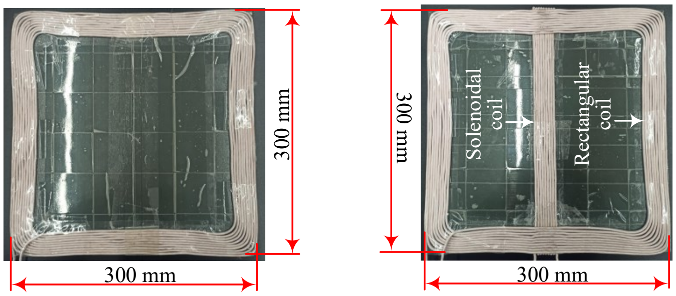

(a) Tx retangular coil pad (b) Rx rectangular-solenoidal pad

Fig. 12. Top view of the Tx retangular coil pad and the Rx rectangular-solenoidal pad (RSP).

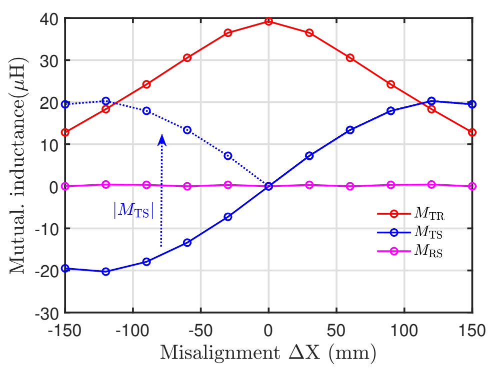

Fig. 13. Mutual inductance polarity of RSP coupler.

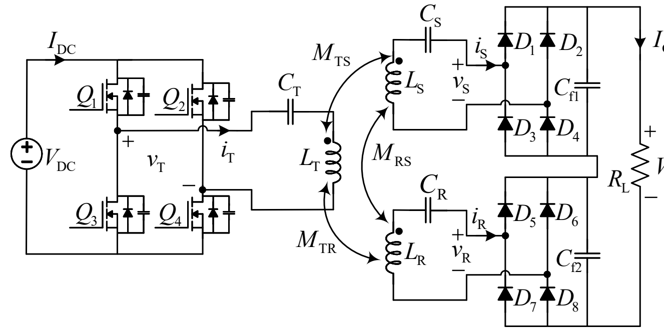

Fig. 14. IPT system with proposed RSP coupler.

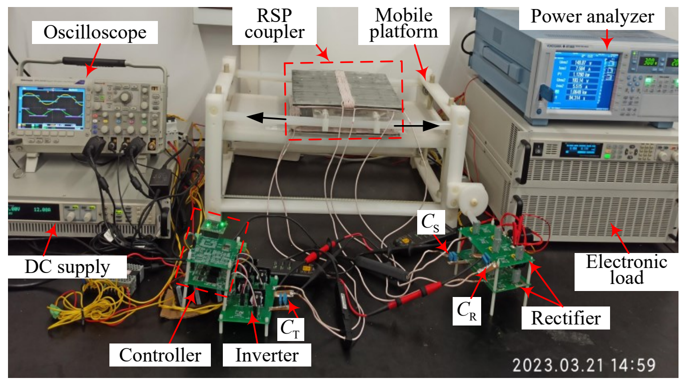

Fig. 15. Experimental prototype of 1-kW IPT system with RSP coupler.

As a comparison, the DDQP coupler has an identical rectangular coil to the proposed RSP, and it also features similar characteristics as the proposed RSP, as shown in Fig. 10. Thus, the design of the DD coil can adopt a similar procedure as shown in Fig. 9. To be concise, the design is not repeated here. With the data shown in Fig. 10 and the values of the slope α_{TDD} versus the turn number N_D are calculated and summarized in Table II, the optimal design locates at $\alpha_{TDD} = 0.163$ by using 6 turns for the DD coil.

B. Copper Usage Analysis

Considering the geometries illustrated in Fig. 6, the lengths of the wires are reliant on the number of turns for both the solenoidal coil and the DD coil, and they are mathematically expressed by

$$L_{S_{tatol}} = 2(L_{RS} + H_{RS})N_S \tag{17}$$

$$\begin{aligned} L_{DD_{tatol}} &= 2\sum_{1}^{N_D} 2(L_{RDD_i} + W_{RDD_i}) \\ &= -8{N_D}^2 + 2(L_{RDD} + 2W_{RDD} + 4d_C)N_D. \end{aligned} \tag{18}$$

With (17) and (18), the copper usage (wire length) versus the turn number is shown in Fig. 11. It can be readily known that the copper usage of the DD coil is 10080 mm, while the solenoidal coil only needs 5670 mm as shown in Fig. 11 and Table II. Therefore, the proposed RSR coupler can save 43.73% litz wire consumption with the same misalignment tolerance.

IV. Experimental Verification

A. Experimental Setup

A magnetic coupler is constructed with a Tx rectangular coil and a Rx RSP coil as shown in Fig. 12. The parameters of the magnetic coupler are summarized in Table I. Moreover, the material of the ferrite core is 3C95, which has permeability $\mu = 3000$ and can be used to realize power transformers for frequencies up to 0.5 MHz. The geometry is plate type with size being $50 \times 50 \times 3$ mm^3. Thus, the magnetic core for the Tx and Rx pads consists of 6×6 pieces of ferrite core and the overall size is $300 \times 300 \times 3$ mm^3. As shown in Fig. 13, the mutual inductance (M_{TS}) exhibits opposite polarities in $+$X and $-$X axis, as depicted by the solid blue curve.

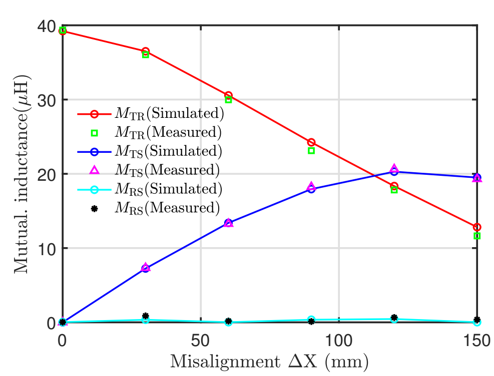

Fig. 16. Measured mutual inductance of proposed RSP coupler versus misalignments along X-axis.

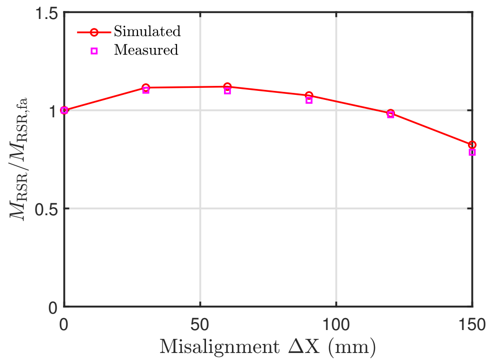

Fig. 17. Normalized mutual inductance M_{RSP} with $N_{\mathrm{S}} = 9$ under different X-misalignments.

Taking this characteristic into account, an IPT circuit topology independent of mutual inductance polarities is developed and depicted in Fig. 14. MOSFETs Q_1-Q_4 form a full bridge inverter responsible for modulating the dc voltage V_{DC} into a high-frequency square wave voltage V_{T}. On the Tx side, diodes D_1-D_4 constitute a purely passive full-bridge rectifier, rectifying the induced ac output current of the solenoidal coil. Similarly, diodes D_5-D_8 establish another rectifier to convert the induced AC output current of the rectangular coil. The outputs of these two rectifiers are in series connection and such a configuration effectively resolves the polarity issue of the M_{TS} without compromising the output characteristic of the IPT system, which is conceptually akin to considering the absolute value of M_{TS}, as indicated by the blue dotted line in Fig. 13. All coils are series compensated, representing a most simplified scheme. L_{T}, L_{R}, and L_{S} are the self-inductances of Tx coil, Rx rectangular coil, and Rx solenoidal coil respectively, while C_{T}, C_{R}, and C_{S} are the corresponding compensation capacitors. The equivalent load of the IPT charging system is modeled as a resistor and determined by the output voltage V_{O} and output current I_{O}, as given by $R_L = \frac{V_{\mathrm{O}}}{I_{\mathrm{O}}}$.

In the design, the solenoidal coil is perpendicular to the rectangular coil, individually capturing the horizontal magnetic flux and vertical magnetic flux respectively. Such that theoretically there is no mutual coupling between them, i.e., M_{RS} = 0. It can also be validated by simulated mutual inductance between these two coils as shown in Fig. 13. Therefore, the DC output current of the IPT system is given by

$$I_{\mathrm{O}} = \frac{8}{\pi^2}\frac{V_{\mathrm{DC}}}{\omega(|M_{\mathrm{TS}}| + |M_{\mathrm{TR}}|)}. \quad (19)$$

It can be observed that the output current is load-independent if $|M_{\mathrm{TS}}|+|M_{\mathrm{TR}}|$ is constant. It should be noted that misalignment tolerance is enabled by the magnetic coupler design, which means it does not rely on the compensation design. Compensation design is subject to the desired output. For example, SS compensation is used in the proposed WPT system for nearly constant current output against misalignment, while LCC-S compensation can achieve nearly constant voltage output against misalignment.

To validate the aforementioned analysis, a 1-kW prototype using the proposed RSP coupler is constructed, as depicted in Fig. 15, based on the schematic shown in Fig. 14. The physical dimensions of the RSP coupler are determined using the parameters provided in Table I and the design methodology outlined in Section III, as illustrated in Fig. 12. The system operates at 85 kHz, maintaining a fully resonant state. Consequently, the compensation capacitors C_{T}, C_{S}, and C_{R} are calculated according to the established methods [29], as detailed in Table III. The input dc voltage V_{DC} is set to 150 V, while the fully aligned mutual inductance $M_{\mathrm{RSR,fa}}$ is 39.65 μH. Using (19), the necessary output current I_{O} is computed as 5.7 A. To simulate the misalignment scenario relevant to electric vehicles, an ABS-made mobile platform simulating a vehicle chassis is employed, as shown in Fig. 15.

TABLE III
MEASURED PARAMETERS OF THE IPT PROTOTYPE

Coupler parameters		Circuit parameters	
Symbols	Value	Symbols	Value
L_{T}	101.78 μH	C_{T}	34.4 nF
L_{R}	101.32 μH	C_{R}	34.6 nF
L_{S}	107.22 μH	C_{S}	32.6 nF
$M_{\mathrm{RSR,fa}}$	39.65 μH	R_{L}	30.8 Ω
N	10	V_{DC}	150 V
N_{S}	9	D_1 -D_8	MBR20200CTG
h_{gap}	60 mm	Q_1 -Q_4	STC 4050

B. Measurement of Mutual Inductances Against Misalignment

The measured mutual inductances (i.e., M_{TR}, M_{TS}, and M_{RS}) of the proposed RSP coupler under different misalignments along the X-axis, based on the design results of Section III, are shown in Fig. 16. It can be observed that the mutual inductance M_{TR} decreases while the M_{TS} increases within a range of misalignments. The mutual inductance M_{RS} is almost equal to zero, i.e., $M_{\mathrm{RS}} \approx 0$. As a result, the solenoidal coil and rectangular coil on the receiver side are magnetically decoupled. Fig. 17 presents the measured ratio of equivalent mutual inductance M_{RSR} and the mutual inductance at fully aligned state $M_{\mathrm{RSR,fa}}$ with $N_{\mathrm{S}} = 9$ versus various offsets along X-axis. The measured M_{TR}, M_{TS}, M_{RS}, and $M_{\mathrm{RSP}}/M_{\mathrm{RSP,fa}}$ in Figs. 16 and 17 agree with the simulated results, which verify the above analysis and design method. Moreover, the null coupling phenomenon does not exist within the nominated operating range, i.e., $\pm 50\%$ of the proposed RSP length.

C. Misaglignment-Tolerant of Output Performance

Fig. 18 shows the experimental waveforms of modulated voltage V_{T}, input current i_{T}, induced voltage V_{S}, induced current i_{S}, induced voltage V_{R}, induced current i_{R}, and output current I_{O} at misalignments ΔX=0 mm (fully aligned), ΔX=50 mm, and ΔX=100 mm. It is evident that the output current almost maintains at 5.7 A. More details of the output current I_{O} are plotted in Fig. 19. In Fig. 19, the X-axis misalignment ranges from -150 mm to +150 mm, which means that the maximum misalignment is about 50% of the proposed RSP length. The output current I_{O} is from 5.25 A to 6.32 A, and thus the current fluctuation is within 10.8%.

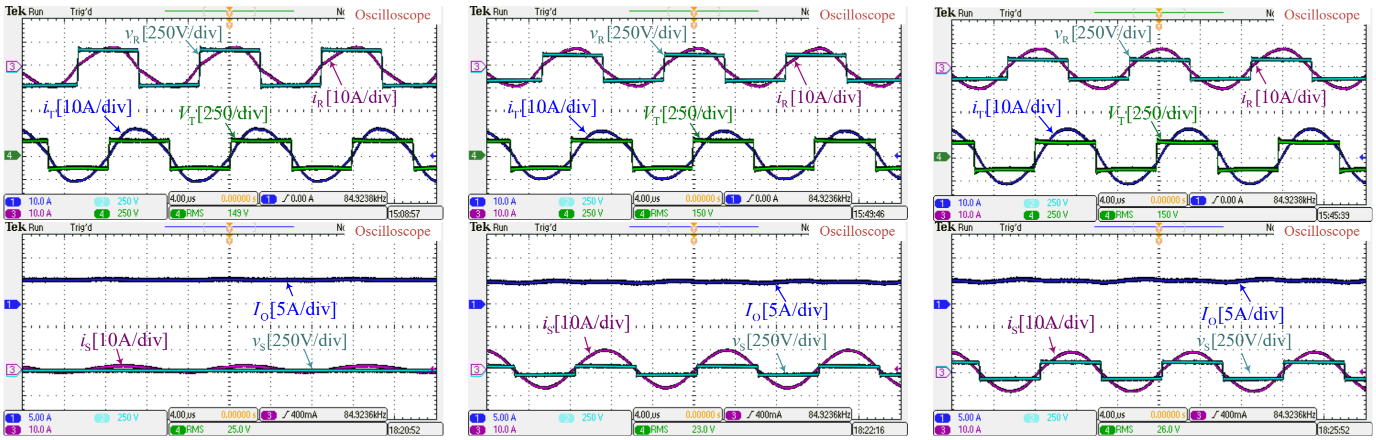

(a) ΔX=0 mm (fully aligned) (b) ΔX=50 mm (c) ΔX=100 mm

Fig. 18. Experimental waveforms of the proposed IPT charging system with RSP at various misalignment conditions: (a) ΔX = 0 mm (fully aligned), (b) ΔX = 50 mm, and (c) ΔX = 100 mm.

TABLE IV
COMPARISON WITH EXISTING WORKS

Type	Citation	Coupler type	Copper usage	Cross-coupling elimination	Additional control	Power transfer capacity	Pad size & Misalignment (cm) (percentage)	Output fluctuation	Efficiency (Fluctuation)
Symmetric design	[7]	CP – CP	Low	Unnecessary	No	Normal	28×14-28×14 &+12(42%)	87.5%	Not considered
	[12]	RP – RP	Low	Unnecessary	No	Normal	40×30-40×30 &+12(30%)	55.1%	78% (15%)
Asymmetric design	[18]	RP matrix– SP	High	Difficult	Yes	Normal	45×30-20×10 & +16 (35.6%)	≤ 8.6%	91% (1%)
	[21]	DDP – DDP	High	Unnecessary	No	Normal	75×50-32×25 & +7.5 (10%)	Not considered	90% (3%)
Anti-series design	[23]	CP&RP – RP	High	Difficult	No	Reduced	30&45×45-40×40 & +18 (40%)	≤ 5%	92% (1%)
	[24]	4 RP – RP	High	Difficult	No	Reduced	45×45-40×40 & +22.5 (50%)	≤ 31.6%	91.1% (16.1%)
	[25]	SDDP – SDDP	High	Difficult	No	Reduced	20.9 ×25-20.9×25 & ±14 (67%)	≤ 6%	91.3% (1.1%)
Proposed design		RP – RSP	Low	Simple	No	Enhanced	30×30-30×30 & ±15 (50%)	≤ 10.8%	94.71% (1.7%)

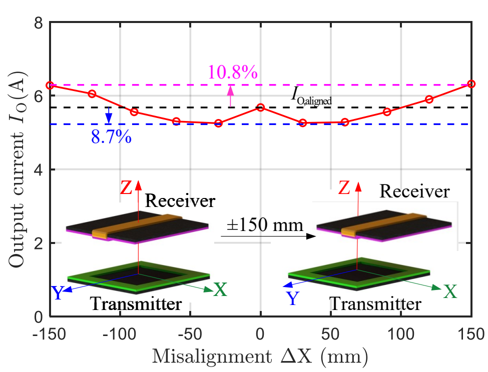

Fig. 19. Output current of proposed IPT system under different misalignments along X-axis.

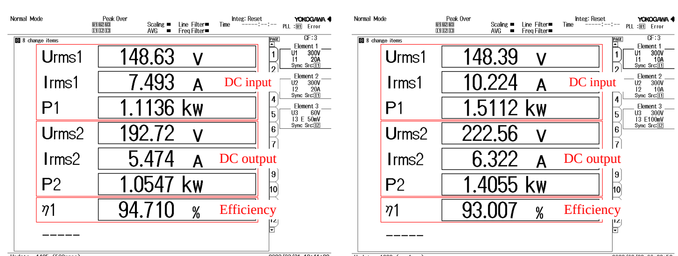

(a) ΔX=0 mm (b) ΔX=150 mm

Fig. 20. Measured power efficiency at various misalignment conditions.

The power efficiency is measured by a power analyzer YOKOGAWA WT1803E, as shown in Fig. 20. The efficiencies at ΔX=0 mm (fully aligned) and ΔX=150 mm (50% of the proposed RSP length) are 94.71% and 93.007%, respectively. As shown in Fig. 21, the efficiency can be maintained high (above 93%) regardless of the misalignment due to the suppression of magnetic flux variation.

D. Discussion

To demonstrate the superiority of the proposed design, a comparison is made between the performance of the proposed method and that of other techniques, as highlighted in Table IV. Compared with the symmetric design using traditional couplers [7], [12], the proposed coupler can achieve an excellent pad misalignment tolerance. The existing asymmetric designs

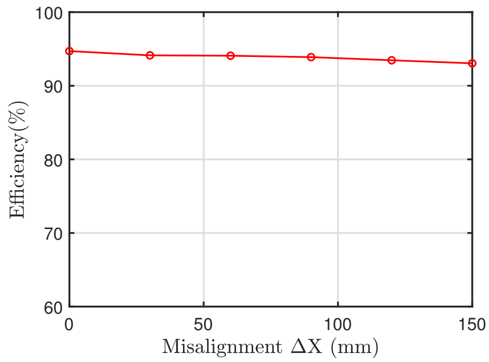

Fig. 21. Measured transfer efficiency of proposed IPT under different misalignments along the X-axis.

[18], [21] and anti-series designs [23]–[25] can improve the capability of misalignment tolerance. However, the penalties of these coupler designs are increased copper usage and degraded power efficiency. Moreover, cross-coupling problems are difficult to alleviate for these designs. In this paper, we consider these problems and develop the proposed misalignment-tolerant design based on the mutual complementary operating principle of mutual inductances. The power transfer capacity can thus be enhanced.

V. Conclusion

To enhance the misalignment tolerance of inductive power transfer (IPT) systems for electric vehicle (EV) charging, this paper introduces a novel IPT coupler that excels in suppressing magnetic flux variation and minimizing copper usage. The proposed coupler, named the rectangular-solenoidal pad (RSP), integrates a rectangular coil and a solenoidal coil, combining the advantages of unipolar and bipolar coils. Compared to the commonly-used double D quadrature pad (DDQP), the RSP demonstrates superior performance in capturing effective magnetic flux linkages while reducing copper usage by 43.73% for misalignment tolerance. The paper utilizes finite element analysis (FEM) to develop a computational method for calculating effective magnetic flux in loosely coupled systems with ferrite magnetic cores under misalignment conditions. Furthermore, the paper details a misalignment tolerance design methodology employing approximate slope predictions for mitigating magnetic field fluctuations. A 1-kW experimental prototype IPT system utilizing the RSP coupler is constructed and tested for validation. Experimental results show that the output current fluctuation is within 10.8% when the misalignment is approximately 50% of the RSP coupler length and the efficiency can be maintained above 93%.

References

[1] G. A. Covic and J. T. Boys, "Inductive power transfer," *Proc. IEEE*, vol. 101, no. 6, pp. 1276–1289, Jun. 2013.

[2] R. Bosshard and J. W. Kolar, "Inductive power transfer for electric vehicle charging: Technical challenges and tradeoffs," *IEEE Power Electron. M.*, vol. 3, no. 3, pp. 22–30, Sept. 2016.

[3] Z. Zhang, H. Pang, A. Georgiadis, and C. Cecati, "Wireless power transfer–an overview," *IEEE Trans. Ind. Electron.*, vol. 66, no. 2, pp. 1044–1058, Feb. 2018.

[4] D. Wang, X. Qu, Y. Yao, and P. Yang, "Hybrid inductive-power-transfer battery chargers for electric vehicle onboard charging with configurable charging profile," *IEEE Trans. Intell. Transp. Syst.*, vol. 22, no. 1, pp. 592–599, Jan. 2021.

[5] A. Mostafa, Y. Wang, H. Zhang, C. Zhu, Y. Mei, N. Jiao, and F. Lu, "Output power regulation of a series-series inductive power transfer system based on hybrid voltage and frequency tuning method for electric vehicle charging," *IEEE Trans. Ind. Electron.*, vol. 69, no. 10, pp. 9927–9937, Oct. 2021.

[6] Z. Huang, S. C. Wong, and C. K. Tse, "Control design for optimizing efficiency in inductive power transfer systems," *IEEE Trans.Power Electron.*, vol. 33, no. 5, pp. 4523–4534, May 2018.

[7] K. Aditya, V. K. Sood, and S. S. Williamson, "Magnetic characterization of unsymmetrical coil pairs using archimedean spirals for wider misalignment tolerance in IPT systems," *IEEE Trans. Transp. Electrif.*, vol. 3, no. 2, pp. 454–463, Jun. 2017.

[8] Z. Luo and X. Wei, "Analysis of square and circular planar spiral coils in wireless power transfer system for electric vehicles," *IEEE Trans. Ind. Electron.*, vol. 65, no. 1, pp. 331–341, Jan 2018.

[9] W. Zhang, J. C. White, A. M. Abraham, and C. C. Mi, "Loosely coupled transformer structure and interoperability study for EV wireless charging systems," *IEEE Trans.Power Electron.*, vol. 30, no. 11, pp. 6356–6367, Nov. 2015.

[10] A. Zaheer, G. A. Covic, and D. Kacprzak, "A bipolar pad in a 10-kHz 300-W distributed IPT system for AGV applications," *IEEE Trans. Ind. Electron.*, vol. 61, no. 7, pp. 3288–3301, July 2014.

[11] M. Mohammad, S. Choi, Z. Islam, S. Kwak, and J. Baek, "Core design and optimization for better misalignment tolerance and higher range of wireless charging of phev," *IEEE Trans. Transport. Electrific.*, vol. 3, no. 2, pp. 445–453, Jun. 2017.

[12] G. Rituraj and P. Kumar, "A new magnetic structure of unipolar rectangular coils in WPT systems to minimize the ferrite volume while maintaining maximum coupling," *IEEE Trans. Circuits Syst. II, Exp. Briefs*, vol. 68, no. 6, pp. 2072–2076, Jun. 2021.

[13] J. Rahulkumar, R. Narayanamoorthi, P. Vishnuram, C. Balaji, T. Gono, T. Dockal, R. Gono, and P. Krejci, "A review on resonant inductive coupling pad design for wireless electric vehicle charging application," *Energy Rep.*, vol. 10, pp. 2047-2079, Nov. 2023.

[14] J. Rahulkumar, R Narayanamoorthi, P. Vishnuram, M. Bajaj, V. Blazek, L. Prokop, and S. Misak, "An empirical survey on wireless inductive power pad and resonant magnetic field coupling for in-motion ev charging system," *IEEE Access*, vol. 11, pp. 4660-4693, Jan. 2023.

[15] G. Rituraj, B. K. Kushwaha, and P. Kumar, "A unipolar coil arrangement method for improving the coupling coefficient without ferrite material in wireless power transfer systems," *IEEE Trans. Transp. Electrif.*, vol. 6, no. 2, pp. 497–509, Mar. 2020.

[16] M. Budhia, G. A. Covic, and J. T. Boys, "Design and optimization of circular magnetic structures for lumped inductive power transfer systems," *IEEE Trans.Power Electron.*, vol. 26, no. 11, pp. 3096-3108, Nov. 2011.

[17] H. Khalid, S. Mekhilef, M. Mubin, M. Seyedmahmoudian, A. Stojcevski, P. Darvish, and A. Hossain, "Design and analysis of a new inductive coil with improved characteristics than conventional magnetic couplers," *IEEE Trans.Power Electron.*, doi: 10.1109/TTE.2023.3313671.

[18] S. A. Al Mahmud, I. Panhwar, and P. Jayathurathnage, "Large-area free-positioning wireless power transfer to movable receivers," *IEEE Trans. Ind. Electron.*, vol. 69, no. 12, pp. 12807–12816, Dec. 2022.

[19] P. Jayathurathnage, Y. Liu, and J. Kyyra, "Self-decoupled and integrated coils for modular multitransmitter wireless power transfer systems," *IEEE Trans.Power Electron.*, vol. 37, no. 11, pp. 12962–12967, Nov. 2022.

[20] W. Zhang, S. C. Wong, C. K. Tse, and Q. Chen, "An optimized track length in roadway inductive power transfer systems," *IEEE J. Emer. Sel. Top. Power Electron.*, vol. 2, no. 3, pp. 598–608, Sept. 2014.

[21] K. Song, G. Yang, Y. Guo, Y. Lan, S. Dong, J. Jiang, and C. Zhu, "Design of dd coil with high misalignment tolerance and low EMF emissions for wireless electric vehicle charging systems," *IEEE Trans.Power Electron.*, vol. 35, no. 9, pp. 9034–9045, Sept. 2020.

[22] J. Shin, S. Shin, Y. Kim, S. Ahn, S. Lee, G. Jung, S. J. Jeon, and D. H. Cho, "Design and implementation of shaped magnetic-resonance-based wireless power transfer system for roadway-powered moving electric vehicles," *IEEE Trans. Ind. Electron.*, vol. 61, no. 3, pp. 1179–1192, March 2014.

[23] Y. Chen, R. Mai, Y. Zhang, M. Li, and Z. He, "Improving misalignment tolerance for IPT system using a third-coil," *IEEE Trans.Power Electron.*, vol. 34, no. 4, pp. 3009–3013, Apr. 2019.

[24] P. Zhang, M. Saeedifard, O. C. Onar, Q. Yang, and C. Cai, "A field enhancement integration design featuring misalignment tolerance for wireless EV charging using LCL topology," *IEEE Trans.Power Electron.*, vol. 36, no. 4, pp. 3852–3867, Apr. 2021.

[25] J. Mai, Y. Wang, Y. Yao, M. Sun, and D. Xu, "High-misalignment-tolerant IPT systems with solenoid and double d pads," *IEEE Trans. Ind. Electron.*, vol. 69, no. 4, pp. 3527–3535, Apr. 2022.

[26] Z. Yuan, M. Saeedifard, C. Cai, Q. Yang, P. Zhang, and H. Lin, "A misalignment tolerant design for a dual-coupled lcc-s-compensated WPT system with load-independent cc output," *IEEE Trans.Power Electron.*, vol. 37, no. 6, pp. 7480–7492, Jun. 2022.

[27] M. Budhia, J. T. Boys, G. A. Covic, and C. Y. Huang, "Development of a single-sided flux magnetic coupler for electric vehicle IPT charging systems," *IEEE Trans. Ind. Electron.*, vol. 60, no. 1, pp. 318–328, Jan. 2013.

[28] S. Bandyopadhyay, P. Venugopal, J. Dong, and P. Bauer, "Comparison of magnetic couplers for IPT-based EV charging using multi-objective optimization," *IEEE Trans. Veh. Technol.*, vol. 68, no. 6, pp. 5416–5429, Jun. 2019.

[29] X. Qu, Y. Yao, D. Wang, S. C. Wong, and C. K. Tse, "A family of hybrid IPT topologies with near load-independent output and high tolerance to pad misalignment," *IEEE Trans.Power Electron.*, vol. 35, no. 7, pp. 6867–6877, July 2020.

[30] *Wireless Power Transfer for Light-Duty Plug-in/Electric Vehicles and Alignment Methodology,* J2954_202208, SAE International, 2022.

Hai Xu received the M.S. degree in agricultural engineering from South China Agricultural University, Guangzhou, China, in 2019. He is currently pursuing the Ph.D. degree in mechanical engineering with Shien-Ming Wu School of Intelligent Engineering, South China University of Technology, Guangzhou, China.

His research interests include wireless power transfer, magnetic coupler design, magnetic modeling, and electric vehicle charging.

Zhicong Huang (Senior Member, IEEE) received the B.Eng. degree in electrical engineering and automation and the M.Eng. degree in mechanical and electronic engineering from the Huazhong University of Science and Technology, Wuhan, China, in 2010 and 2013, respectively, and the Ph.D. degree in power electronics from The Hong Kong Polytechnic University, Hong Kong, in 2018.

He is currently an Associate Professor with the Shien-Ming Wu School of Intelligent Engineering, South China University of Technology, Guangzhou, China. His research interests include power electronics techniques in electric vehicles and power systems. Dr. Huang received the Outstanding Reviewer Award from IEEE Transactions on Power Electronics in 2021.

Xiaolu Lucia Li (M'20) received the B.Eng. and M.Phil. degrees in electrical engineering from the Harbin Institute of Technology, China, in 2014 and 2016, respectively, and the Ph.D. degree in power electronics from Hong Kong Polytechnic University, Hong Kong, in 2019. She is currently a Postdoctoral Fellow with the Department of Electrical Engineering, City University of Hong Kong. Her research interests include multiport converters and wireless power transfer.

Chi K. Tse (M'90–SM'97–F'06) received the BEng (Hons) degree with first class honors in electrical engineering and the PhD degree from the University of Melbourne, Australia, in 1987 and 1991, respectively.

He is presently Associate Vice President (Innovation), Director of the Academy of Innovation, and Chair Professor of Electrical Engineering at City University of Hong Kong, Hong Kong. His research interests include power electronics, nonlinear systems and complex network applications.

He was the recipient of a number of research and invention prizes including the IEEE CASS Charles A. Desoer Technical Achievement Award in 2022 and a few Best Paper Prizes from IEEE and other journals, as well as a Grand Prize and Gold Medal in Silicon Valley International Invention Festival 2019. He has been appointed to honorary professorship and distinguished fellowship by a few Australian, Canadian and Chinese universities, including the Chang Jiang Scholar Chair Professor with Huazhong University of Science and Technology, Honorary Professor of Melbourne University, and Distinguished Professor-at-Large with the University of Western Australia. He also served as panel member of Hong Kong Research Grants Council, and member of several professional and government committees.

In 2005, 2010 and 2018, he was selected as an IEEE Distinguished Lecturer. In 2006 he chaired the IEEE CAS Technical Committee on Nonlinear Circuits and Systems. He serves and has served as Editor-in-Chief of IEEE Transactions on Circuits and Systems II (2016-2019), IEEE Circuits and Systems Magazine (2013-2016), IEICE Nonlinear Theory and Applications (since 2013); as associate editor of a few other IEEE journals; and on the Editorial Board of IEEE Proceedings (2021-2022). He has served on a number of IEEE committees including the IEEE Fellows Committee and the IEEE Awards Committee, and chaired the Steering Committee for IEEE Transactions on Network Science and Engineering.